ELSEVIER

PII: S0032-3861(98)00134-7

Polymer Vol. 39 No. 125, pp. 6205–6211, 1998

0032-3861/98/$ - see front matter

Probing the gelation of polymers within a Bentheimer sandstone by ^{1}H-PFG n.m.r.

E. W. Hansen[a,*], Kjell Olafsen[b] and Per Olav Kvernberg[c]
[a]*SINTEF Applied Chemistry, P.O. Box 124 Blindern, N-0314, Norway*
[b]*SINTEF Materials Technology, P.O. Box 124 Blindern, N-0314 Oslo, Norway*
[c]*UiO, P.O. Box 1033 Blindern, N-0314 Oslo, Norway*
(Accepted 5 January 1998)

The gelation of a polyvinylalcohol–glutaraldehyde–water solution confined in a Bentheimer sandstone was characterized by carrying out ^{1}H-n.m.r. spin-lattice relaxation rate measurement ($1/T_1$) and pulse field gradient diffusion (D) measurements at 67°C. At any time during the gel reaction neither the longitudinal magnetization *versus* storage time nor the echo-amplitude *versus* gradient strength (squared) could be described by single exponential functions. In order to characterize these multi-exponential decay curves by a minimum number of parameters a gaussian type of distribution function (Rayleigh distribution) in $1/T_1$ and D were adopted. When implementing these distribution functions and fitting all spin-lattice relaxation data and diffusion data simultaneously, in order to constrain the fitting more effectively, the two n.m.r. derived parameters ($1/T_1$ and D) were found to give consistent results. During gelation the average relaxation rate and the average diffusion coefficient *versus* reaction time were found to be described by a first order rate process with a rate constant equal to $18 \times 10^{-5}\,s^{-1}$. Also, the widths of the two distribution functions were found to decrease with reaction time. Moreover, the gelation rate within the Bentheimer sandstone was found to be significantly faster compared to the gelation rate of the bulk solution.

(Keywords: polyvinyl alcohol; glutaraldehyde; gel)

INTRODUCTION

High-viscosity polymeric fluids and gels have been used to control the water mobility and the water profiles in injectors, with the primary application in enhanced oil recovery[1–4]. In recent years, interest has been focused on using biopolymers as gelation agent because of their non-toxic and environmental advantages[2]. To extract information related to the mechanisms and the kinetics involved in this type of reaction systems, a number of different experimental techniques have been used[5–7]. ^{1}H-n.m.r. relaxation time measurements have been applied successfully to study the kinetics of gelation processes involving paramagnetic ions (chromium)[8,9]. However, chromium is a rather controversial chemical due its potential toxic hazards. Therefore, a non-toxic gel system composed of polyvinylalcohol (PVA) and glutaraldehyde dissolved in saline water was later investigated by Hansen *et al.*[10] using conventional ^{1}H-n.m.r. spectroscopy. This reaction was investigated in bulk solution giving rise to narrow resonance lines from the reagent and product molecules which could be monitored *versus* reaction time. Variable temperature measurements enabled both mechanistic and kinetic parameters to be extracted.

Recently, Hansen *et al.*[11] showed that using the pulsed field gradient (PFG) n.m.r. technique it was possible to follow the gelation process of PVA not only in bulk solution but also within a porous 'material' composed of glass beads. Due to the multi-exponential behaviour of the observed n.m.r. signal intensity *versus* the square of the applied gradient field, a simple and unique physical representation of the gelation process was complex.

The object of the present work is therefore to introduce a more rigorous physical model based on a distribution coefficients to account for the observed multi-exponentiality of the observed n.m.r. signal intensity. Moreover, an improved data analysis which constrains the fitting more effectively will be discussed. Both diffusion measurements and spin-lattice relaxation time measurements will be reported and related to the rate of gelation. Also, a more convenient and natural porous material (Bentheimer sandstone) is chosen in this study, rather than the more artificial porous material composed of packed glass beads as reported[11].

EXPERIMENTAL

Materials

The reagents used in this study were Floperm 665P (polyvinyl alcohol) from OFPG Inc., Floperm 665X1 (25% glutaraldehyde in eater) from OFPG Inc., and a brine solution with a total ionic strength of 0.475. All chemicals were used as received without further purification. The pH of the bulk solution was approximately 4.7. To mimic the porous system normally found in oil reservoirs we selected a Bentheimer sandstone which, from experience, contains a minimum amount of paramagnetic and ferromagnetic salts. Porous materials containing such salts have a devastating effect on the n.m.r. signal due to a significant shortening of the spin–spin relaxation times, resulting in an unwanted increase in the decay rate of the transversal magnetization. The porous material was cut to a small cylindrical piece of length approximately 15 mm and a diameter of approximately 4 mm which nicely fits in to the 5 mm n.m.r. tube. The pore size is in the range of a few microns. No cleaning

* To whom correspondence should be addressed

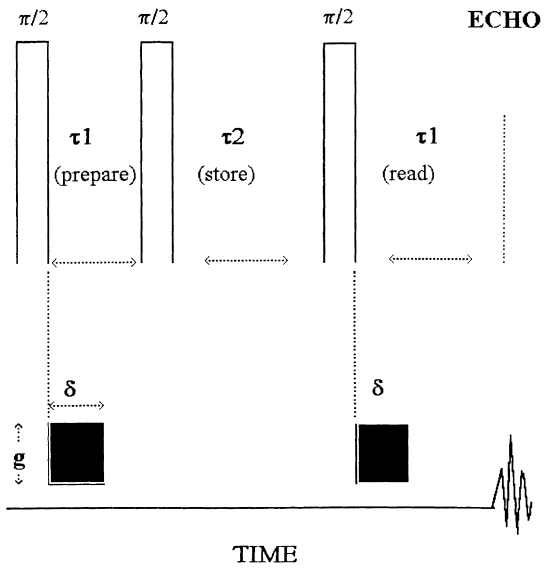

Figure 1 Schematic drawing of the pulsed field gradient stimulated echo pulse sequence. Symbols are defined in the text

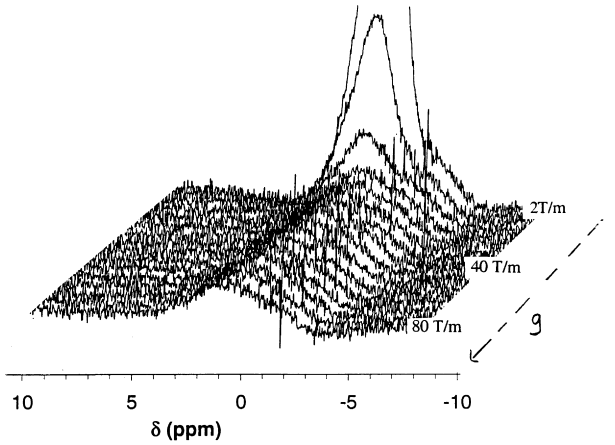

Figure 2 ^{1}H-n.m.r. spectra versus the strength of the field gradient pulse (g) at the end of the gelation process ($t = 8.4$ h). The low field resonance band corresponds to the methine proton and the high field band correspond to the methylene protons in PVA

or pretreatment was applied except that the plug was stored at 105°C overnight before being saturated with the polymer solution.

Preparation of solution

352 μl of crosslinker was mixed with 100 g of the premade gel solution and stirred for 5 min at room temperature. No significant gelation was initiated at this temperature[10,11]. The sandstone was filled with the gel mixture under vacuum and transferred to a 5 mm n.m.r. tube. The n.m.r. tube was sealed before transferred to the magnet at 80°C where the n.m.r. measurement was initiated.

The diffusion measurements were all performed on a Bruker DMX 200 AVANCE operating at 200 MHz using a spin-lattice stimulated spin-echo pulse field gradient technique[12–15]. The pulse sequence is illustrated in *Figure 1*, showing three successive $\pi/2$ r.f.-pulses with a time delay of τ_1 (preparation time) between the first two pulses and a time delay τ_2 (storage time) between the second and the last pulse. The $\pi/2$ pulse was 5.2 μs. The second part of the figure (below) shows the gradient pulses characterized by their duration (δ) and strength (g). The echo is observed at time τ_1 after the last r.f.-pulse. If not stated otherwise in the text the following parameters were used; $\delta = 2$ ms, $\tau_1 = 2.5$ ms, $\tau_2 = 15.5$ ms. The spin-lattice relaxation time (T_1) was measured using the same pulse sequence with a constant gradient pulse strength of 200 gauss cm^{-1} and by varying the storage time τ_2; 10, 20, 40, 80, 160, 320, 640 and 1280 ms. The time between transients was set to more than five times the spin-lattice relaxation time to ensure quantitative measurements.

A Bruker diffusion probe denoted MIC DIF 200 WB was used in all experiments.

THEORY

The pulsed field-gradient pulse sequence, which is illustrated in *Figure 1*, facilitates the measurement of D in systems in which the spin-lattice relaxation time (T_1) is large relative to the spin–spin relaxation time (T_2), as is often the case in polymer systems[16].

The echo intensity (I) can be represented by:

$$I = \sum_i M_{0i} R_1(\tau_2; T_{1i}) \cdot R_2(\tau_1; T_{2i}) \cdot R_3(\tau_1, \tau_2, g; D_i) \quad (1a)$$

where;

$$R_1(\tau_2; T_1) = \exp(-\tau_2/T_1) \quad (1b)$$

$$R_2(\tau_1; T_1) = \exp(-\tau_1/T_2) \quad (1c)$$

$$R_3(\tau_1, \tau_2, \delta, g; D) = \exp(-(\gamma\delta g)^2 \cdot (\tau_1 + \tau_2 - \delta/3) \cdot D) \quad (1d)$$

where γ is the magnetogyric ratio equal to 2.67×10^8 s^{-1} T^{-1}. The other symbols have been defined previously (see also *Figure 1*).

RESULTS AND DISCUSSION

Preliminary

The single pulse ^{1}H-n.m.r. spectra (not shown) of the PVA–glutaraldehyde–water solution confined in a Bentheimer sandstone revealed a single, non-resolved broad peak with no fine structure. The more than two orders of magnitude larger line width of the solvent water resonance peak within the porous material as compared to the line width in bulk solution is mainly caused by the magnetic susceptibility difference between the solid matrix (Bentheimer) and the confined water. This significant broadening of the water peak masks any observable resonance peaks arising from the polymer (PVA) due to its much lower concentration (1–2 mass%) and made it experimentally impossible to remove the water peak by, for instance, homo-decoupling[12] or by use of any solvent suppression technique[17]. Recognizing that the diffusion coefficients of water and polymer are expected to be significantly different, and that the diffusion of the polymer molecules will decrease during crosslinking/gelation, the use of the PFG n.m.r. technique is the ultimate choice[11].

Figure 2 shows the ^{1}H-n.m.r. spectrum of the polymer solution confined in a Bentheimer sandstone approximately 10 h after the solution was initiated into the sandstone. Gradient pulses larger than 200 gauss cm^{-1} were applied to ensure that the signal from the more mobile water molecules is reduced to zero. The remaining n.m.r. signal intensity originates from the polymer only. The rather broad resonance is composed of two resonance bands, corresponding to the methine protons (low field) and the methylene

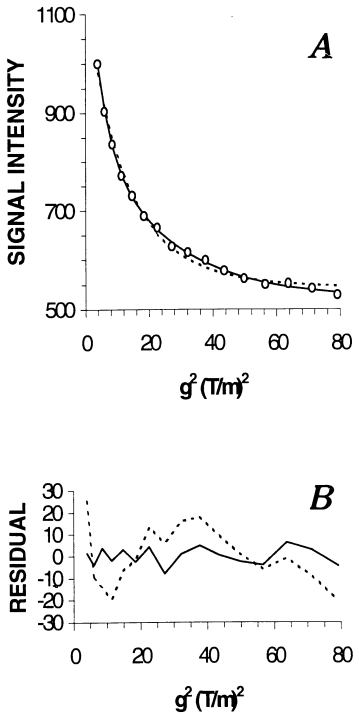

Figure 3 (A) PFG n.m.r. echo signal intensity (area) *versus* the square of the field gradient pulse (g^2) of PVA (*Figure 2*) at the initial stage of the gel reaction ($t = 0.93$ h). The solid/dotted curves represent three-exponential and two-exponential fits to the observed echo intensity. (B) Residuals from the exponential fits shown in *Figure 3a*. See text for further details

protons (high field) of PVA[11]. Due to susceptibility broadening, the resonance band is difficult to deconvolute. In this work we have therefore used the area of the complete resonance band to represent the n.m.r. signal intensity of PVA.

Diffusion

The feasibility of eliminating the large solvent water signal by the PFG technique makes it possible to follow changes in the polymer during the gel reaction. Also, the n.m.r. parameters T_1, T_2 and the self-diffusion coefficient (D) can be monitored *versus* reaction time when applying this particular n.m.r. technique, i.e. observing the echo decay signal under different experimental conditions. With reference to equation (1), the echo-intensity *versus* the gradient strength squared (g^2) at any given time during the gelation process (when T_1 and T_2 are constants) will be purely exponential if τ_1, τ_2 and δ are kept constant and the polymer is described by a single diffusion coefficient.

Figure 3 shows the echo intensity of PVA *versus* the gradient strength squared (g^2) at time $t = 56$ min after placement of the gel solution within the Bentheimer sandstone. According to the constraints just outlined, equation (1) simplifies to;

$$I = \sum_i M'_{0i} \cdot \exp[-(\gamma\delta)^2(\tau_1 + \tau_2 - \delta/3)D \cdot g^2] \qquad (2)$$

where the parameter $M'_{0i} = M_{0i} \cdot R_1 \cdot R_2$ is constant.

Equation (2) was fitted to the observed echo-intensity curve. Using statistical validity tests, the numerical analysis showed a best fit to the observed decay curve to be represented by three diffusion coefficients; $D_1 = (6.5 \pm 1.5) \times 10^{-7}$ cm^2 s^{-1}, $D_2 = (4.6 \pm 1.7) \times 10^{-8}$ cm^2 s^{-1} and $D_3 = (2.5 \pm 1.9) \times 10^{-9}$ cm^2 s^{-1} with M'_{0i} equal to 28%, 25% and 47%, respectively (*Figure 3A*; solid curve). If fitting only two exponentials to the observed echo curve (*Figure 3a*; dotted curve), the diffusion coefficients changes to $D_1 = (2.42 \pm 0.18) \times 10^{-7}$ cm^2 s^{-1} and $D_2 = (5.81 \pm 0.73) \times 10^{-9}$ cm^2 s^{-1} with relative intensities of 46% and 54%, respectively. In this latter case, however, the residuals of the fit reveals a non-random error distribution, as shown in *Figure 3B* (dotted curve). The cognition of three diffusional components giving a best fit to the observed echo intensity was found to be of genuine nature at all reaction times (1–9). The smaller diffusion coefficient was found, within experimental error, to be constant with reaction time and more than an order to magnitude smaller than the two larger diffusion coefficients. The smaller diffusion coefficient, of the order of 10^{-9} cm^2 s^{-1}, represents a limiting value regarding sensitivity, i.e. slower diffusional motion can not be resolved by the present PFG technique. We have recently[11] pointed out the complication involved in rationalizing the observation of three time dependent diffusion coefficients. Noting, however, that the two larger diffusion coefficients are rather close to each other and that the third coefficient is much longer and independent of reaction time, the analysis can be simplified by introducing a distribution of diffusion coefficients ($w(D)$) for the faster diffusion process. This implies that the overall diffusion process of the polymer can be characterized by a bimodal distribution in D, where one diffusion mode can be approximated by a slow and time independent diffusion process. The origin of a distribution of diffusion coefficients is related to the molecular weight distribution which has been discussed by many authors[18–20]. In the next section we will introduce the concept of distribution and derive a mathematical model which will implement this idea in relation to the PFG measurements.

Interlude

Regarding the accuracy of the diffusion coefficient obtained in this work, one should consider the effect of susceptibility and restricted motion (pore confined fluid) on the echo-signal intensity *versus* gradient field strength squared (g^2). The average distance (r) a molecule diffuses between the first and second gradient pulse ($t = 18$ ms) can be approximated by the well known Einstein equation; $r^2 = 6Dt$, where D is the diffusion coefficient. This gives $r < 1$ μm which is less than the pore dimension of the material investigated and suggests that pore restriction only has a minor effect on the measured diffusion coefficient. Regarding the effect of susceptibility on the derived diffusion coefficient this is a more complicated and complex matter. This effect can, however, be partly overcome by applying a more sophisticated pulse sequence[21]. In this work, we are essentially not concerned about the absolute value of D but rather the relative change in D *versus* reaction time. Thus, no further consideration or action regarding minimisation of the susceptibility effect on the echo signal intensity *versus* gradient strength is taken in this work.

Distribution of diffusion coefficients

A large number of continuous distribution functions exist of which the most frequently used are; Binomial, Gaussian, Poisson, Gamma, Rayleigh, Weibull, Maxwell, Log–normal and Beta distributions[22]. We have no a priori knowledge of what type of distribution which will represent the distributions of D. Our choice will simply be dictated by mathematical simplicity and the object of obtaining a simple analytical solution for the n.m.r. echo-signal intensity. Often

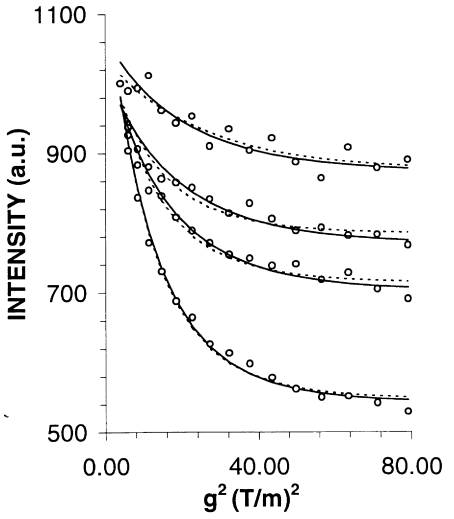

Figure 4 Echo signal intensity *versus* the square of the gradient pulse (g^2) at different times during the reaction. From bottom to top; $t = 0.93$, 1.85, 2.78, 5.56 h. The solid curves represent individual fits of Equation (5) to the data while the dotted curves represent corresponding fits to all experimental data, i.e. both the spin-lattice relaxation rate data (see *Figure 6*) and diffusion data (*Figure 4*). See text for further details

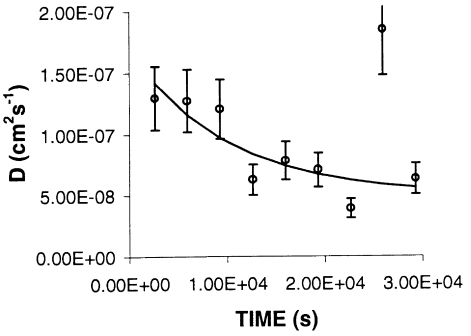

Figure 5 The self-diffusion coefficient of the fast diffusion mode ($D_{\text{distr.}}$) *versus* reaction time. The solid curve is derived by model fit as explained in the text

a log–normal distribution is used to characterize molecular weight distributions[20]. However, this particular type of distribution function will result in a rather complicated and non-analytical solution to our specific problem. A modified Gaussian distribution function denoted the Rayleigh distribution which takes the form;

$$w(x) = x \cdot \exp\left[-\left(\frac{x - x_0}{\sqrt{2}\sigma}\right)^2\right] \tag{3}$$

has therefore been chosen. In this equation x represents the independent variable, x_0 is the average value and σ is the width of the distribution. The advantage of this function compared to the gaussian distribution function is that it forces $w(x)$ to 0 for $x = 0$ which is a physically adequate constraint. Also, this function leads to the reasonable result that $w(x) = 0$ for $x = \infty$.

Considering the exponential behaviour of the diffusional term in equation (1) with respect to D, the average values of R_3 can be written;

$$R_{\text{av}(3)} = \int_0^\infty D\exp\left[-\left(\frac{D - D_0}{\sqrt{2}\cdot\sigma_D}\right)^2\right]\cdot\exp(-\beta\cdot D)\,\mathrm{d}D \tag{4}$$

where the parameter β is equal to $(\tau_1 + \tau_2 - \delta/3)\cdot(\gamma\delta g)^2$. After some tedious algebra, the following expression for $R_{\text{av}(3)}$ can be derived (see Appendix);

$$R_{\text{av}(3)} = \exp(\sigma_D^2\beta^2/2 - D_0\beta)\cdot\left\{\sigma_D^2\cdot\exp\left[\frac{D_0 - \sigma_D^2\beta}{\sqrt{2}\sigma_D}\right] + \sqrt{2}\sigma_D(D_0 - \sigma_D^2\beta)\cdot erfc\left[\frac{\sigma_D^2\beta - D_0}{\sqrt{2}\sigma_D}\right]\right\} \tag{5}$$

where 'erfc' is a conventional shorthand notation for the complementary error function defined by;

$$erfc(u) = \int_u^\infty \exp(-u^2)\,\mathrm{d}u$$

We emphasize that $2N$ parameters are needed to fit N discrete diffusion coefficients to equation (1) while only three parameters are needed when introducing the Rayleigh distribution function. Thus, introducing the distribution function approach has the effect of increasing the number of degrees of freedom in the curve-fitting procedure. Moreover, the exponential character of all the R-functions in equations (1a), (1b), (1c) and (1d) makes it possible to derive average values of these R-functions which are analogous to equation (5) when applying the same kind of distribution functions (Rayleigh functions) to characterize the distribution in $1/T_1$ and $1/T_2$. We simply replace the parameter β with τ_2 and τ_1 and the parameter σ_D with $\sigma_{1/T1}$ and $\sigma_{1/T2}$, respectively, in equation (5).

As mentioned earlier in this section, we have implicitly assumed that the distribution of diffusion coefficients of the polymer can be described by a bimodal distribution in which the first mode is represented by a single and slow diffusion component (which is independent of reaction time) while the other mode is represented by a Rayleigh distribution (equation (5)) with a much shorter diffusion component. PFG experiments were run at nine different times (t) during the gelation process ($t = 0.92$, 1.85, 2.78, 3.71, 4.64, 5.57, 6,49, 7.42 and 8.34 h) and the echo intensities fitted to the above outlined model. For the purpose of clarity only four of these results are illustrated in *Figure 4* where the dotted curves represent model fits to equation (5). The solid curves will be discussed in the next section. The resulting average diffusion coefficients of the faster diffusion mode of all the nine experiments are shown in *Figure 5 versus* reaction time. The solid curve represents a model fit which will be discussed in the next two sections.

Spin-lattice relaxation rate

Application of the spin-echo pulse sequence enables the spin-lattice relaxation time (T_1) to be determined by varying the storage time τ_2 while keeping τ_1 and the gradient strength (g) constant. It has to be emphasized that this approach necessitates the knowledge of the self-diffusion coefficient (D), as can be inferred from equation (1). Assuming the spin-lattice relaxation rate ($1/T_1$) to be characterized by a Rayleigh distribution function (equation (3)) we can easily show that the following model equation will apply to this T_1 experiment;

$$I = M'_{01}R_{\text{av}(2)}(\tau_2; T_{1,\text{distr}})\cdot R_{\text{av}(3)}, (\tau_1, \tau_2, g; D_{\text{distr.}}) + M'_{02}R(\tau_2; T_{1,\text{long}})\cdot R_3(\tau_1, \tau_2, g; D_{\text{long}}) \tag{6}$$

where $R_{\text{av}(2)}$ is identical to equation (5) with β replaced by τ_1 and D_0 and σ_D replaced by $1/T_1$ and $\sigma_{1/T1}$, respectively.

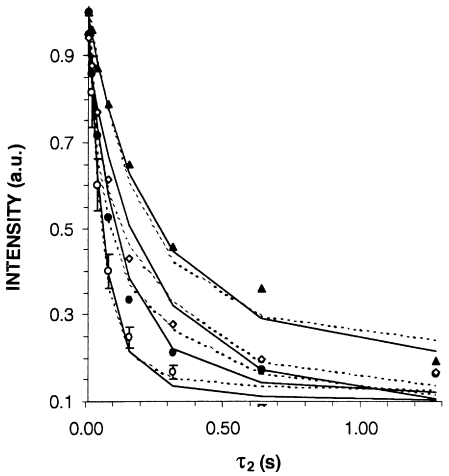

Figure 6 Signal intensity *versus* time (τ_2) obtained from the PFG n.m.r. pulse sequence during reaction time (t). From bottom to top; $t = 0.93$, 1.85, 2.78, 5.56 h. The solid curves represent individual fits of Equation (5) to the data while the dotted curves represent corresponding fits to all experimental data, i.e. both the spin-lattice relaxation rate data (*Figure 6*) and diffusion data (*Figure 4*). See text for further details

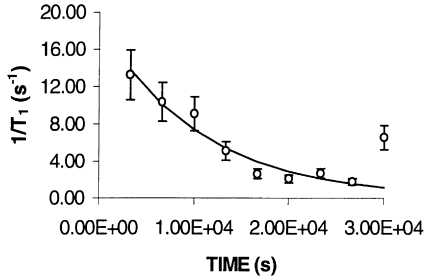

Figure 7 Spin-lattice relaxation rate ($1/T_{1,\mathrm{distr}}$) *versus* reaction time. The solid curve is derived by model fit as explained in the text

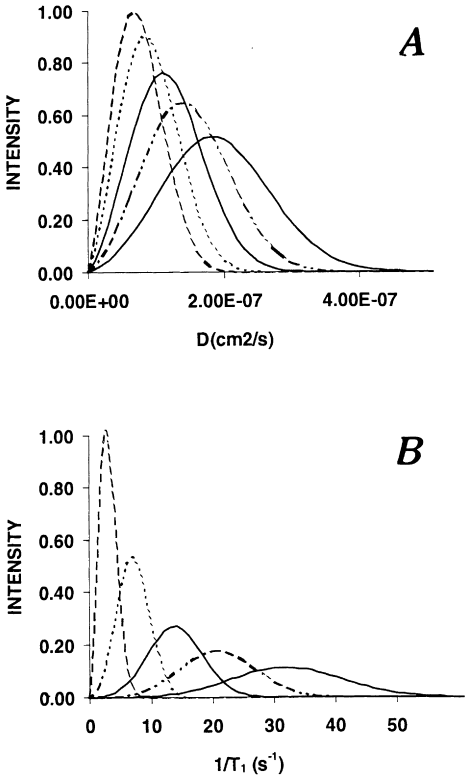

Figure 8 Model calculated distribution functions of (A) the overall diffusion coefficient and (B) the spin-lattice relaxation rate of PVA *versus* reaction time (t). From right to left the reaction times used in the calculations are $t = 0.0.56$, 1,11, 2.22 and 27.5 h. See text for further details

$R_{av}(3)$ is equal to equation (1). Moreover, M'_{0i} ($i = 1,2$) are constants which only vary with reaction time (t) due to a potential change in T_2 *versus t*. $D_{1\mathrm{long}}$ has been shown to be constant and independent on reaction time and equal to 2.5×10^{-9} cm^2 s^{-1}. Using the previously derived D_{distr} values (*Figure 5*), equation (6) was fitted to the observed echo-signal *versus* time (τ_2) at nine specific times (t) during the reaction. For the sake of clarity, only four of these data sets with corresponding model fits (dotted curves) are shown in *Figure 6*. The single relaxation time $T_{1,\mathrm{long}}$ was found to be, within experimental error, constant and equal to 1600 $\pm$ 900 ms. The derived average relaxation rates $1/T_{1,\mathrm{distr}}$ of the fast diffusion mode *versus* reaction time are plotted in *Figure 7*. The solid curves represents model fits and will be discussed in the next section.

Improvement and consistency in model fitting—gelation rate

The fitting of the diffusion data (*Figure 4*, dotted curves) and the relaxation data (*Figure 6*, dotted curves) have been performed with a minimum set of data points. In order to access the extrinsic value of the gelation rate and to constrain the fitting more effectively, an obvious extension of the data analysis would be to consider all diffusion data and all relaxation data as a single data matrix. This can be realized by assuming the gelation rate (k) to be equivalent to the rate of change in the spin-lattice relaxation rate *versus* reaction time and to the change in the rate of the overall diffusion *versus* reaction time.

In mathematical terms we will thus assume that the rate of change in both spin-lattice relaxation and diffusion will follow a first order rate law, i.e.

$$Y = [Y_0 - Y_\infty]\cdot\exp(-kt) + Y_\infty \qquad (7)$$

where Y can be identified as the spin-lattice relaxation rate ($1/T_1$) or the self-diffusion coefficient (D). Y_0 and Y_∞ represents the initial Y-value (at the start of the reaction) and the equilibrium Y-value (at the end of the reaction), respectively.

The analysis discussed above has indicated that the distribution parameters $\sigma_{1/T1}$ and σ_D follow a similar trend (not shown) *versus* reaction time as the spin-lattice rate and the self-diffusion coefficient. To further constrain the model fit we will thus assume that the spread (σ) in these distribution parameters follow the same first order dependence *versus* reaction time, as described by equation (7). Based on these assumptions, the whole data matrix (216 data points) has been fitted to equations (5) and (6) under the constraints represented by equation (7). The results are shown by the solid curves in *Figures 4, and 6* and by the solid curves in *Figures 5, and 7*. As can be seen, this simultaneous three-dimensional fit (I *versus* g^2, τ_2 and reaction time t), under the above constraints, gives a very good representation of the complete data set with a rate of gelation of the order of $k = 18 \times 10^{-5}$ s^{-1} at 67°C. The results of the parameter fit are summarized in *Table 1*. This rate of gelation is of the same order of magnitude as the gelation found in a porous model system composed of glass beads (20×10^{-4} s^{-1}) as determined by an equivalent n.m.r. approach[11]. However, the gelation rate is, within experimental error, almost an order of magnitude larger than the corresponding gelation rate observed in bulk solution using a somewhat different n.m.r. approach[10].

Table 1 Rate constant (k) and characteristics of the distribution functions (Rayleigh distribution function; Equation (3)) of the spin-lattice relaxation rate ($1/T_1$) and the self-diffusion coefficient (D) during an expected first order gelation process (Equation (7)) at 80°C. The parameters are derived by fitting the model equation (Equation (1)) to the complete set of relaxation data and diffusion data from a PFG n.m.r. experiment (see text for further details)

X	$1/T_1$ (s^{-1})	D ($cm^2\ s^{-1}$)
$\sigma^0 x$	5.8	2.5×10^{-8}
$\sigma^\infty x$	1.7	5.1×10^{-8}
X_0	25	9.0×10^{-8}
X_∞	2.3	7.6×10^{-8}
k_x (s^{-1}) [a]	18×10^{-5}	18×10^{-5}

σ_x^0 and σ_x^∞ represent the width of the distributions at the start and at the end of the gel reaction, respectively. Likewise, X_0 and X_∞ define the average value of the distributions at the start and at the end of the gel reaction. X is a shorthand notation for D and $1/T_1$

[a] The change in spin-lattice relaxation and self-diffusion *versus* reaction time has been constrained in the model fit, i.e. $k_{1/T1} = k_D$

These results suggest that the gelation within a porous material proceeds faster than in bulk solutions and indicate that interactions between the pore surface and the polymer solution might affect the gelation rate. It is reasonable to expect that this latter interaction will be of less importance with increasing pore dimension. This needs further investigation.

In order to visualize the change in diffusion rate and spin-lattice relaxation rate of the fast diffusion mode of PVA during gelation, the distribution functions of these parameters are plotted at five different times during the reaction (*Figure 8*). As can be inferred from this figure both parameters are initially very broad. With increasing time, both the diffusion rate and the spin-lattice relaxation rate decrease and become more narrow. This suggests that the molecules combine due to crosslinking and diffuse more slowly and uniformly (due to the decreasing width of the distribution) with reaction time.

Assuming the translational correlation time to be dominated by dipole–dipole interactions, the decrease in spin-lattice relaxation rate would, according to the Bloembergen–Purcell–Pound (BPP)[23] model, cause an increase in the overall translational correlation time. This is in agreement with the increasing crosslinking during the gel reaction which reduces the mobility of the molecules. These observations suggests an intimate correlation between the overall diffusion and the molecular translational correlation time.

An interesting aspect of the n.m.r. analysis is to monitor the change in the relative amount of polymer molecules associated with the 'fast' diffusion mode *versus* reaction time. In order to derive this information, the spin–spin relaxation rates have to be measured (see equation (1)). This is a somewhat more tricky exercise, due to J-modulation[16]. However, the use of a modified stimulated spin-echo pulse sequence denoted the pulsed field-gradient longitudinal eddy-current delay pulse sequence (PFGLED)[16] should accomplish this and will be the subject of future studies.

CONCLUSION

In this work we have shown that the gelation of a polymer–crosslink–water system confined in a porous sandstone (Bentheimer) can be probed by application of a PEG n.m.r. technique. Introducing a distribution of diffusion coefficients and a distribution of spin-lattice relaxation rates show that the polymer can be divided into two modes of molecular motion, a 'fast' and a 'slow' mode of motion. The derived theoretical model used to fit the experimental n.m.r. data suggests an intimate correlation between the diffusion coefficient and the spin-lattice relaxation rate of PVA. The gelation rate, as characterized by the change in the fast mode of motion of the polymer *versus* reaction time, proceeds significantly faster within a porous material as compared to a bulk polymer solution, and is tentatively explained by a pore surface–polymer interaction.

ACKNOWLEDGEMENTS

We would like to thank NFR, Norsk Hydro, Total, Schlumberger, Dyno, Saga and Borregaard and Akzo-PQ for financial support, and Prof. Bjørn Pedersen at the UiO for permitting us to perform the diffusion measurements.

APPENDIX

In this section we will assume that a measurable parameter y depends exponentially on a n.m.r. parameter x according to an exponential relation;

$$y = I_0 \exp(-\beta \cdot x) \tag{A1}$$

If the parameter x is varying within the system under investigation we might approximate this variation by introducing a distribution function $w(x)$. Based on physical reality we will assume that $w(0) = w(\infty) = 0$. A large number of distribution functions satisfying these constraints exist. We will, however, limit the following discussion to one particular distribution function, the Rayleigh distribution function defined by;

$$w = x \cdot \exp\left[-\left(\frac{x - x_0}{\sqrt{2}\sigma}\right)^2\right] \tag{A2}$$

where x_0 represents the average value of x and σ the width of the distribution. Inserting this distribution function into equation (A1) enables the average value (y_{av}) of the observable y to be derived from equation (A3);

$$y_{av} = I_0 \int_0^\infty x \cdot \exp\left[-\left(\frac{x - x_0}{\sqrt{2}\sigma}\right)^2\right] \cdot \exp(-\beta \cdot x)\, dx \tag{A3}$$

Rearrangement of the exponential terms gives;

$$y_{av} = I_0 \cdot [\sigma^2\beta^2/2 - x_0\beta] \cdot \int_0^\infty x \cdot \exp\left[-\left(\frac{x + \sigma^2\beta - x_0}{\sqrt{2}\sigma}\right)^2\right] dx \tag{A4}$$

The integral on the left side can be simplified by substituting

$$u = \frac{x + \sigma^2\beta - x_0}{\sqrt{2}\sigma} \Leftrightarrow du = \frac{1}{\sqrt{2}\sigma} dx \tag{A5}$$

into equation (A4), which results in the following expression;

$$y_{av} = I_0\sqrt{2}\sigma\cdot\exp[\sigma^2\beta^2/2 - x_0\beta]\cdot\left[\sqrt{2}\sigma\int_{(\sigma^2\beta - x_0)/\sqrt{2}\sigma}^{\infty}[u\exp(-u^2) + (x_0 - \sigma^2\beta)\exp(-u^2)]\,du\right] \quad \text{(A6)}$$

The first integral term in equation (A6) can be solved by partial integration resulting in the following and final expression for the average value of y;

$$y_{av} = I_0\exp(\sigma^2\beta^2/2 - x_0\beta)\cdot\left\{\sigma^2\cdot\exp\left[\frac{x_0 - \sigma^2\beta}{\sqrt{2}\sigma}\right] + \sqrt{2}\sigma(x_0 - \sigma^2\beta)\cdot erfc\left[\frac{\sigma^2\beta - x_0}{\sqrt{2}\sigma}\right]\right\} \quad \text{(A7)}$$

where 'erfc' is a conventional shorthand notation for the complementary error function defined by $erfc(u) = \int_0^{\infty}\exp(-u^2)\,du$ which is a tabulated function. Equation (A7) is identical to equation (5).

REFERENCES

1. Sorbie, K. S., Parker, A., Clifford, P. J., *SPE Reservoir Engineering*, 1987, August, 281.
2. Chauveteau, G. and Kohler, N., SPE 9295, presented at the *1980 SPE Annual Technical Conference and Exhibition*, Dallas, TX, September 21–24.
3. Needham, R. B., Threlkeld, C. B., Gall, J. W., SPE 4747, presented at the *Improved Oil Recovery Symposium of the SPE of AIME*, Tulsa, OK, April 22–24, 1974.
4. Batycky, J. P., Maini, B. B., Milosz, G., *SPE 6th International Symposium On Oilfield and Geothermal Chemistry*, Dallas, TX, January 25–27, 1982.
5. Prud'homme, R. K., Uhl, J. T., Poinsatte, J. P., Halverson, F., *SPEJ Soc. Pet. Eng. J.*, 1983, 804.
6. Prud'homme, R. K., Uhl, J. T., Poinsatte, J. P., Halverson, F., *SPEJ Soc. Pet. Eng. J.*, 1984, **24**, 121.
7. Lund, T., Smidsrød, O., Stokke, B. T. and Elgsaether, F., *Carbohydr. Polym.*, 1988, **8**, 245.
8. Hansen, E. W. and Lund, T., *J. Phys. Chem.*, 1991, **95**, 341.
9. Hansen, E. W. and Lund, T., *J. Phys. Chem.*, 1995, **99**, 1995.
10. Hansen, E. W., Holm, K. H., Jahr, D. M., Olafsen, K. and Stori, Aa., *Polym.*, 1996, **38**, 4295.
11. Hansen, E. W., Olafsen, K., Klaveness, T. M. and Kvernberg, P. O., *Polymer*, 1998, **39**, 1279.
12. Harris, R. K., *Nuclear Magnetic Resonance Spectroscopy, a Physical Review*. Pitman Books Limited, London, 1983.
13. Tanner, J. E., *J. Chem. Phys.*, 1970, **52**, 2523.
14. Haase, A. and Frahm, J., *J. Magn. Res.*, 1985, **65**, 481.
15. Cotts, R. M., Hoch, M. J. R., Sun, T. and Markert, J. T., *J. Magn. Res.*, 1989, **83**, 252.
16. Waldeck, A. R., Kuchel, P. W., Lennon, A. J. and Chapman, B. E., *Progr. Nucl. Magn. Res.*, 1997, **30**, 39.
17. Hore, P. J., *J. Magn. Res.*, 1983, **55**, 283.
18. Raghavan, R., Maer, T. L. and Blum, F. D., *Macromol.*, 1987, **20**, 814.
19. Fleicher, G., *Polymer*, 1985, **26**, 1677.
20. Chen, A., Wu, D. and Johnson, C. S. Jr., *J. Am. Chem. Soc.*, 1995, **117**, 7965.
21. Søland, G. H., Diffusion measurements in heterogeneous Media, Ph.D. thesis, Dep. Phys. Chem., NTNU, Trondheim (Norway), 1997.
22. Spiegel, M. R., *Statistics, Schaum's Outline Series*. McGraw-Hill book Company, New York, 1972.
23. Bloembergen, N., Purcell, E. M. and Pound, R. V., *Phys. Rev.*, 1948, **73**, 679.